



Imaginary-time relaxation quantum critical dynamics in the two-dimensional dimerized Heisenberg model

Jia-Qi Cai,¹ Yu-Rong Shu,² Xue-Qing Rao ¹ and Shuai Yin ^{1,*}

¹*Guangdong Provincial Key Laboratory of Magnetolectric Physics and Devices, School of Physics, Sun Yat-sen University, Guangzhou 510275, China*

²*School of Physics, Guangzhou University, Guangzhou 510275, China*



(Received 17 March 2024; revised 16 April 2024; accepted 18 April 2024; published 6 May 2024)

We study the imaginary-time relaxation critical dynamics of the Néel paramagnetic quantum phase transition in the two-dimensional dimerized $S = \frac{1}{2}$ Heisenberg model. We focus on the scaling correction in the short-time region. A unified scaling form including both short-time and finite-size corrections is proposed. According to this full scaling form, improved short-imaginary-time scaling relations are obtained. We numerically verify the scaling form and the improved short-time scaling relations for different initial states using projector quantum Monte Carlo algorithm.

DOI: [10.1103/PhysRevB.109.184303](https://doi.org/10.1103/PhysRevB.109.184303)

I. INTRODUCTION

Quantum phase transitions (QPTs) describe nonanalytic changes between different ground states of many-body systems [1]. Although QPTs are governed by quantum fluctuations at zero temperature, they can remarkably influence the finite-temperature phase diagram, giving rise to a variety of exotic behaviors in the famous quantum critical regime as exhibited in a wide range of strongly correlated systems [1,2]. Thus, the QPTs have received considerable attention from both theoretical and experimental aspects. Among various models of QPTs, the $S = \frac{1}{2}$ Heisenberg antiferromagnet has attracted enormous investigations [3–23], not only because it is one of the typical quantum models whose ordered phase can spontaneously break continuous symmetry, but also owing to its close relation to strongly correlated materials such as the cuprate superconductors [13,24–26].

Recent investigations on QPTs are increasingly focusing on their nonequilibrium dynamics because the interplay between the divergent correlation timescale and the breaking of the translation symmetry in time direction can trigger lots of intriguing universal dynamic behaviors, which usually go beyond the conventional scheme of equilibrium QPTs [27–42]. For example, in equilibrium, quantum criticality in d dimensions can usually be mapped into the corresponding classical criticality in $(d + 1)$ dimensions via the path-integral formulation [1,2]. In contrast, there is no similar mapping between quantum and classical critical dynamics for the nonequilibrium case. Aside from the theoretical novelty, intriguing nonequilibrium critical phenomena have been found in various experiments [43–48]. Moreover, quantum critical dynamics also has important applications in preparing and characterizing various exotic quantum phases in fast-developing quantum devices [49–53].

In addition to the real-time dynamics, imaginary-time dynamics in quantum systems are also of great interest and significance. Because of its dissipative nature, the imaginary-time evolution typically serves as a reliable unbiased method to determine the ground state, not only widely used in numerical simulations, such as the time-evolving block decimation [54,55], tensor network [56,57], and quantum Monte Carlo (QMC) [14,58,59], but also in rapidly developing quantum computers [60–62]. Near a quantum critical point, universal scaling behaviors have been shown to appear not only in the long-time equilibrium stage, but also in short-time relaxation stage after a transient timescale [63,64]. The short-imaginary-time quantum critical dynamics has been studied extensively in various quantum systems, including the quantum Ising model [63–66], deconfined quantum criticality [67,68], and strongly correlated Dirac systems [69], providing an abundance of intriguing perspectives in the field of quantum criticality. Additionally, the short-imaginary-time scaling behavior has been detected in an experimental platform of a noisy intermediate-scale quantum computer [70]. Moreover, the short-imaginary-time critical dynamics has proven effective in determining critical properties with high efficiency, circumventing difficulties induced by critical slowing down and divergent entanglement entropy encountered in conventional methods based on equilibrium scaling [63–70]. However, the short-imaginary-time scaling property has not yet been explored in the quantum Heisenberg universality class.

In this paper, we explore the imaginary-time relaxation critical dynamics of the Heisenberg universality class in the QPT between Néel antiferromagnetic (AFM) and quantum paramagnetic (PM) states in the two-dimensional dimerized Heisenberg model with interdimer and intradimer couplings J_1 and J_2 , as illustrated in Fig. 1. We find that the relaxation dynamics of this model exhibits scaling behaviors with significant short-time scaling corrections. A unified scaling form that incorporates both short-time and finite-size corrections

*yinsh6@mail.sysu.edu.cn

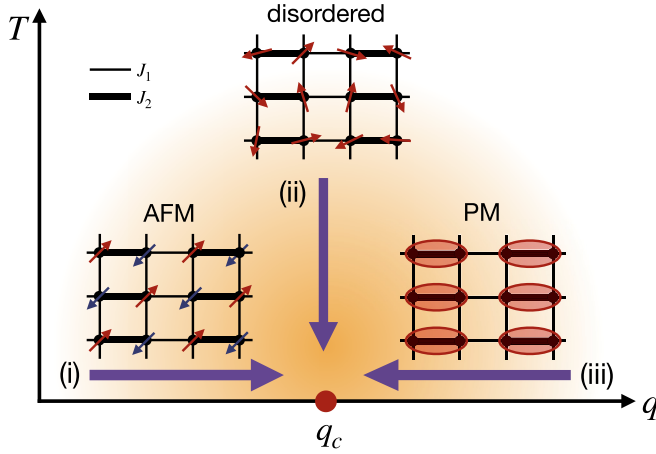


FIG. 1. Sketch of the phase diagram and the quench protocol in imaginary time with different initial states. J_1 and J_2 are the antiferromagnetic coupling on bonds $\langle ij \rangle$ (thin) and $\langle ij' \rangle$ (thick), respectively. The initial states are prepared as (i) the Néel antiferromagnetic phase, (ii) the disordered state, and (iii) the dimerized paramagnetic state. All states correspond to the fixed points of the initial states under the renormalization group transformation.

has been developed. Short-imaginary-time scaling properties with scaling corrections can be inferred from the unified scaling form. For different initial states, we find that the relaxation dynamics in the imaginary-time direction can be well described by this scaling form. The short-time scaling relations are also verified numerically. This work not only reveals the imaginary-time relaxation critical dynamics in the Heisenberg universality class, but also provides a systematic scaling analysis on the scaling corrections in the time direction. These findings can be generalized to other kinds of nonequilibrium critical dynamics.

The rest of the paper is arranged as follows. The dimerized Heisenberg model is introduced in Sec. II. Then, in Sec. III, after a brief review on the original short-imaginary-time scaling theory in Sec. III A, the scaling theory with short-time corrections is developed in Sec. III B. The main numerical results are shown in Sec. IV. At last, a summary is given in Sec. V.

II. MODEL

The Hamiltonian of the 2D dimerized Heisenberg model reads as [3–7,13]

$$H = J_1 \sum_{\langle ij \rangle} \mathbf{S}_i \cdot \mathbf{S}_j + J_2 \sum_{\langle ij' \rangle} \mathbf{S}_i \cdot \mathbf{S}_j, \quad (1)$$

in which $\mathbf{S}_i = (\frac{1}{2})(\sigma_x, \sigma_y, \sigma_z)$ denotes the spin- $\frac{1}{2}$ operator at site i , J_1 and J_2 are the antiferromagnetic coupling constants defined on the bonds $\langle ij \rangle$ and $\langle ij' \rangle$, respectively, as illustrated in Fig. 1. When $q \equiv J_2/J_1 \approx 1$, the ground state of Eq. (1) hosts the Néel AFM order [14,19], characterized by the order parameter $\mathbf{M} \equiv (1/L^2) \sum_r (-1)^{r_x+r_y} \mathbf{S}_r$. In contrast, when $q > q_c = 1.90951(5)$ [19], the ground state changes to the paramagnetic (PM) state. It was shown that the dimerized Heisenberg model can be mapped to a nonlinear sigma model

with an irrelevant Berry phase term and its criticality is well described by the Heisenberg $O(3)$ universality class [3,7,13]. This claim has been verified with scrutiny by numerical simulations via efficient quantum Monte Carlo methods [14].

III. SCALING THEORY IN SHORT-IMAGINARY-TIME QUANTUM CRITICAL DYNAMICS

In this section, after briefly reviewing the short-imaginary-time scaling theory in Sec. III A, we generalize this theory to include the short-time and finite-size scaling corrections, as illuminated in Sec. III B.

A. Brief review on short-imaginary-time quantum critical dynamics

The imaginary-time evolution of a quantum state $|\psi(\tau)\rangle$ is described by the imaginary-time Schrödinger equation

$$-\frac{\partial}{\partial \tau} |\psi(\tau)\rangle = H |\psi(\tau)\rangle, \quad (2)$$

imposed additionally by the normalization condition $\langle \psi(\tau) | \psi(\tau) \rangle = 1$. Its formal solution is $|\psi(\tau)\rangle = Z \exp(-\tau H) |\psi(0)\rangle$, in which $|\psi(0)\rangle$ is the initial wave vector and $Z \equiv 1/\|\exp(-\tau H) |\psi(0)\rangle\|$ is the normalization factor. The expectation value of an operator \hat{Q} at τ is then given by

$$\mathcal{Q}(\tau) = \langle \psi(\tau) | \hat{Q} | \psi(\tau) \rangle. \quad (3)$$

For a gapped quantum system with an arbitrary initial state $|\psi(0)\rangle$, in which $|\psi(0)\rangle$ is assumed to have some overlap with the ground state, the wave function $|\psi(\tau)\rangle$, evolving according to Eq. (2), will fast decay to the ground state after a timescale $\tau_\Delta \sim 1/\Delta$ with Δ being the gap. Based on this, the imaginary-time evolution according to Eq. (2) provides an effective method to find the ground state numerically [14,54–59]. In contrast, when the system is at its critical point, $\Delta \rightarrow 0$ in the thermodynamics limit and thus τ_Δ diverges. This reflects the critical slowing down in quantum phase transitions.

Associated with the divergence of τ_Δ , when the quantum system is near its critical point, nonequilibrium scaling behaviors emerge in the imaginary-time relaxation process. It has been shown that quantum imaginary-time relaxation dynamics exhibits scaling behaviors similar to the classical short-time critical dynamics, as both have a dissipative nature [63,64,71–74].

In analogy with the classical situation [71–74], after a transient period of the microscopic timescale, the operator \mathcal{Q} transforms as [63,64]

$$\mathcal{Q}(\tau, \delta, L, \{Y\}) = b^\kappa \mathcal{Q}(\tau b^{-z}, \delta b^{1/\nu}, L b^{-1}, \{Y_0 b^{-y_0}\}), \quad (4)$$

under a scale transformation with a rescaling factor b . In Eq. (6), κ is the dimension of \mathcal{Q} , $\delta = q - q_c$ is the distance to the critical point and has a dimension of $1/\nu$ with ν being the correlation length exponent, z is the dynamic exponent, and Y_0 with its exponent y_0 denotes the relevant initial information. In contrast to the equilibrium scale transformation [2], here the imaginary time τ is naturally added to describe the nonequilibrium evolution. Besides, the variable of initial state

Y_0 also becomes necessary since the initial information can be remembered for very long timescales as a result of the critical slowing down.

By choosing $b = \tau^{1/z}$ in Eq. (6), one obtains the time-dependent scaling form for \mathcal{Q} [63,64]:

$$\mathcal{Q}(\tau, \delta, L, \{Y\}) = \tau^{\kappa/z} f_Q(\delta \tau^{1/\nu z}, \tau L^{-z}, \{Y_0 \tau^{-y_0/z}\}). \quad (5)$$

In the long-time limit, i.e., $\tau \gg L^z$ and $\tau \gg |\delta|^{-\nu}$, Y_0 vanishes and the usual equilibrium finite-size scaling form is recovered.

In particular, when the initial state corresponds to the fixed point of renormalization group transformation, such as the completely ordered and disordered initial states, the term Y_0 can hide away in Eq. (5). In this way, the scaling form (5) becomes [63,64,71–74]

$$\mathcal{Q}(\tau, \delta, L) = \tau^{\kappa/z} f_{Q1}(\delta \tau^{1/\nu z}, \tau L^{-z}). \quad (6)$$

Note that in this case the detailed function of f_{Q1} still implicitly depends on Y_0 . For example, from the completely ordered initial state, the evolution of the square of the order parameter M^2 at $\delta = 0$ satisfies [63]

$$M^2(\tau, L) = \tau^{-2\beta/\nu z} f_{M1}(\tau L^{-z}), \quad (7)$$

in which β is the order-parameter exponent defined as $M \propto |\delta|^\beta$ in the ordered phase. In the short-time stage, $f_{M1}(\tau L^{-z})$ tends to a constant and

$$M^2 \propto \tau^{-2\beta/\nu z}, \quad (8)$$

whereas in the long-time stage, $f_{M1}(\tau L^{-z}) \propto (\tau L^{-z})^{2\beta/\nu z}$ and scaling form restores to $M^2 \propto L^{-2\beta/\nu}$ [14], which is the leading term of the finite-size scaling form

$$M^2(\tau, L) = L^{-2\beta/\nu} f_{M2}(\tau L^{-z}). \quad (9)$$

In addition, from the completely disordered initial state, M^2 obeys [67,72]

$$M^2(\tau, L) = L^{-d} \tau^{-2\beta/\nu z + d/z} f_{M3}(\tau L^{-z}) \quad (10)$$

for $\delta = 0$. In Eq. (10), $M^2 \propto L^{-d}$ in the leading term comes from the central limit theorem when the correlation length is smaller than L [72]. In the short-time stage, $f_{M3}(\tau L^{-z})$ tends to a constant and

$$M^2 \propto L^{-d} \tau^{-2\beta/\nu z + d/z}, \quad (11)$$

whereas in the long-time stage, $f_{M3}(\tau L^{-z}) \propto (\tau L^{-z})^{2\beta/\nu z - d/z}$, giving rise to $M^2 \propto L^{-2\beta/\nu}$ and Eq. (9).

B. Scaling corrections in short-imaginary-time quantum critical dynamics

The preceding scaling analyses only consider the leading contributions of the relevant scaling variables. However, scaling corrections from the subleading contributions are also very important in characterizing quantum criticality. For example, the finite-size scaling corrections have been shown to play a significant role in determining critical properties in practical numerical simulations [14]. Moreover, figuring out scaling corrections also provides strong evidence to clarify the universality classes of QPTs [14,17–19,75]. Previous investigations mainly focus on the scaling corrections for equilibrium finite-size scaling [14]. For the nonequilibrium critical dynamics,

the time is an intrinsic variable, such that the scaling correction from the time direction is essential and should be carefully accounted for.

For simplicity, in the following, we shall consider the cases for which $\delta = 0$ and initial states are at their fixed points under scale transformation. We start with the general scaling form of a quantity \mathcal{Q} ,

$$\mathcal{Q}(\tau, L) = L^\kappa f_{Q3}(\tau L^{-z}, L^{-\omega_L}, \tau^{-\omega_\tau}), \quad (12)$$

in which $L^{-\omega_L}$ is the usual finite-size scaling correction [14,21] and ω_L is the correction exponent, and $\tau^{-\omega_\tau}$ represents the short-time scaling corrections with ω_τ the correction exponent. In Eq. (12), we assume that $\omega_\tau = \omega_L$ and both of them are denoted as ω . This assumption is based on the fact that the critical theory of the quantum Heisenberg model has the Lorentz symmetry [3–7,13] and will be verified by the numerical results in the next section.

However, directly using the full ansatz (12) is impractical as the detailed form of the scaling function f_{Q3} is unknown. Here, we propose that Eq. (12) can be approximated as

$$\mathcal{Q}(\tau, L) = L^\kappa (1 + b_Q L^{-\omega}) f_{Q4}[\tau L^{-z} (1 + a_Q \tau^{-\omega})], \quad (13)$$

in which b_Q is the coefficient of finite-size correction and equals its equilibrium value, and a_Q is the coefficient of the short-time correction. Both a_Q and b_Q depend on the quantity \mathcal{Q} . In addition, a_Q should also depend on the initial state.

The properties of Eq. (13) are discussed as follows. First, in the long-time limit, i.e., $\tau \rightarrow \infty$, $\tau^{-\omega}$ vanishes and $f_{Q4}(\tau L^{-z})$ tends to a constant. Accordingly, Eq. (13) is reduced to

$$\mathcal{Q}(\tau, L) \propto L^\kappa (1 + b_Q L^{-\omega}), \quad (14)$$

which is consistent with the usual finite-size scaling relation with finite-size scaling correction included [14,19,21].

Second, to reveal the short-time scaling relations, we set $\tau L^{-z} (1 + a_Q \tau^{-\omega}) = c$, namely, $L = [\tau (1 + a_Q \tau^{-\omega}) / c]^{1/z}$ where c is a constant. By substituting this equation into Eq. (13), we obtain

$$\begin{aligned} \mathcal{Q}(\tau, L) &= \tau^{\kappa/z} (1 + a_Q \tau^{-\omega})^{\kappa/z} \\ &\times (1 + b_Q L^{-\omega}) f_{Q5}[\tau L^{-z} (1 + a_Q \tau^{-\omega})], \end{aligned} \quad (15)$$

in which $c^{1/z}$ has been absorbed into f_{Q5} . From Eq. (15), one finds that for large L , the short-time dynamics of \mathcal{Q} satisfies

$$\mathcal{Q}(\tau) \propto \tau^{\kappa/z} (1 + a_Q \tau^{-\omega})^{\kappa/z}. \quad (16)$$

We will illustrate the short-imaginary-time scaling theory with scaling corrections for different quantities. For example, at the critical point $\delta = 0$, with the initial state corresponding to its fixed point, the evolution of the dimensionless Binder cumulant, defined as $U \equiv \frac{5}{2} (1 - \frac{5(M)^4}{3(M^2)^2})$, should satisfy

$$U(\tau, L) = (1 + b_U L^{-\omega}) f_U[\tau L^{-z} (1 + a_U \tau^{-\omega})], \quad (17)$$

according to Eq. (13).

In addition, the square of the order parameter M^2 should obey

$$M^2(\tau, L) = L^{-2\beta/\nu} (1 + b_M L^{-\omega}) f_{M4}[\tau L^{-z} (1 + a_M \tau^{-\omega})]. \quad (18)$$

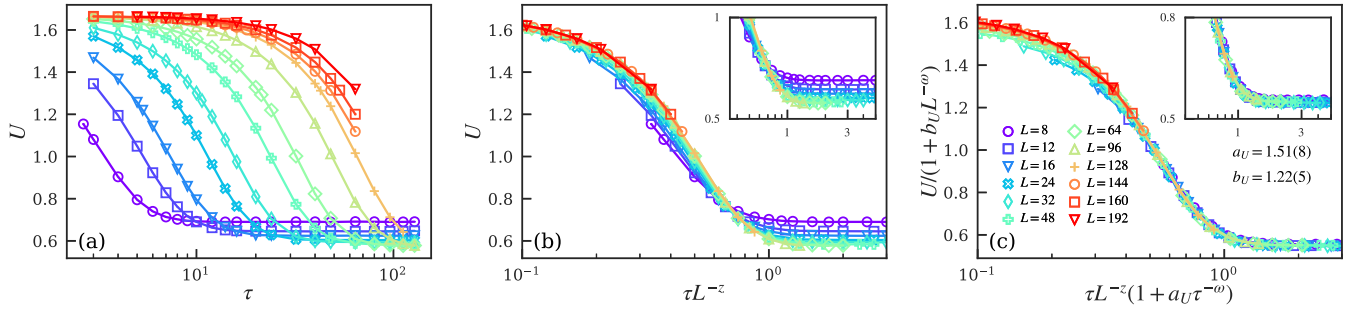


FIG. 2. (a) Evolution of the Binder ratio from the completely ordered initial state for different lattice sizes at the critical point is shown. (b) When τ is rescaled as τL^{-z} , deviations still appear for the rescaled curves of U versus τ . (c) Rescaled curves collapse well when both short-time and finite-size scaling corrections are added. Note that in (c), the correction exponents for both time and size are set as $\omega = 0.78$. Logarithmic scale is used in x axis.

In particular, for an ordered initial state, the evolution of M^2 should follow the scaling form

$$M^2(\tau, L) = \tau^{-2\beta/vz} (1 + a_M \tau^{-\omega})^{-2\beta/vz} \times (1 + b_M L^{-\omega}) f_{M5}[\tau L^{-z} (1 + a_M \tau^{-\omega})], \quad (19)$$

according to Eq. (15). Note that here the dependence of a_M on the initial states is not explicitly shown to avoid complex labels. For large L , Eq. (19) indicates that in the short-time stage

$$M^2(\tau) \propto \tau^{-2\beta/vz} (1 + a_M \tau^{-\omega})^{-2\beta/vz}, \quad (20)$$

according to Eq. (16). Comparing with Eq. (8), one finds that a correction factor has been multiplied. In the next section, we will find that the factor is crucial in describing the short-imaginary-time relaxation dynamics of the model (1).

Moreover, for a disordered initial state, M^2 should obey

$$M^2(\tau, L) = L^{-d} \tau^{-2\beta/vz+d/z} (1 + a_M \tau^{-\omega})^{-2\beta/vz+d/z} \times (1 + b_M L^{-\omega}) f_{M6}[\tau L^{-z} (1 + a_M \tau^{-\omega})]. \quad (21)$$

It is assumed that the leading term of L^{-d} is not affected by the scaling correction since $M^2(\tau, L) \propto L^{-d}$ is a direct result of the probability theory, rather than the result induced by the quantum fluctuations in QPT. For large L , Eq. (21) indicates that in the short-time stage

$$M^2(\tau, L) = L^{-d} \tau^{-2\beta/vz+d/z} (1 + a_M \tau^{-\omega})^{-2\beta/vz+d/z}, \quad (22)$$

according to Eq. (16). Compared to Eq. (11), a scaling correction factor is multiplied here.

IV. RESULTS

A. Numerical method

We employ the projector QMC to implement the imaginary-time relaxation critical dynamics of the model described by Eq. (1). We here briefly outline the method.

To realize the Schrödinger dynamics as introduced in Sec. III A, in the projector QMC method, one takes the series expansion of the imaginary-time evolution operator $U(\tau) = \exp(-\tau H)$ in powers of H^n , and apply to the initial state $|\psi(0)\rangle$, giving $|\psi(\tau)\rangle = \sum_{n=0}^{\infty} \frac{\tau^n}{n!} (-H)^n |\psi(0)\rangle$. After splitting the Hamiltonian into bond operators and inserting unit operators into the operator sequence, the normalization $Z = \langle \psi(\tau) | \psi(\tau) \rangle$ can be importance sampled with the wave

function written in a chosen basis, which is the standard spin- z basis or the valence-bond basis in this work, depending on the initial state desired. The actual expansion power n is truncated to some maximum cutoff length that scales as $L^d \tau$ with vanishing truncation error. A whole Monte Carlo sweep of the important sampling procedure consists of local diagonal updates and global off-diagonal updates, which updates the operator sequence and the basis states simultaneously. The local diagonal updates are performed first, replacing unit operators with diagonal ones at an appropriate acceptance rate and vice versa, within the operator sequence. Then the global operator-loop updates follow up, which switch the operator types between diagonal and correspondingly update the basis states. Detailed balance and ergodicity are maintained. The computational consumption of a full sweep of Monte Carlo update scales as $2\tau L^d$. The update schemes are largely the same as those in the standard stochastic series expansion QMC method [14]. Measurements are carried out in the middle of the double-sided projection, as indicated in Eq. (3). In studies of relaxation dynamics, the initial state of the system is crucial. To realize a specified initial state, the imaginary-time boundaries are held fixed during the updates. In this work, three types of initial states are considered: (i) completely ordered AFM state, (ii) random disordered state, and (iii) dimerized PM state, as shown in Fig. 1. Types (i) and (ii) are implemented in the spin- z basis while type (iii) employs the valence-bond basis so to maintain the dimerized order in the initial state. For a more detailed introduction of the method, we refer to the literature [14,78].

B. AFM initial state

We first investigate the imaginary-time relaxation critical dynamics from the completely ordered AFM initial state.

The dynamics of the dimensionless Binder cumulant is shown in Fig. 2(a). Figure 2(b) shows that although rescaled curves of U versus τL^{-z} for different L tends to collapse in comparison to Fig. 2(a), apparent deviation remains for short-time and small-size cases. Then, we add the scaling corrections and rescale U and τ according to Eq. (17). By tuning a_U and b_U , the rescaled curves are found to collapse very well, as shown in Fig. 2(c). These results demonstrate the necessity of short-time and finite-size scaling corrections in the imaginary-time relaxation dynamics of the model

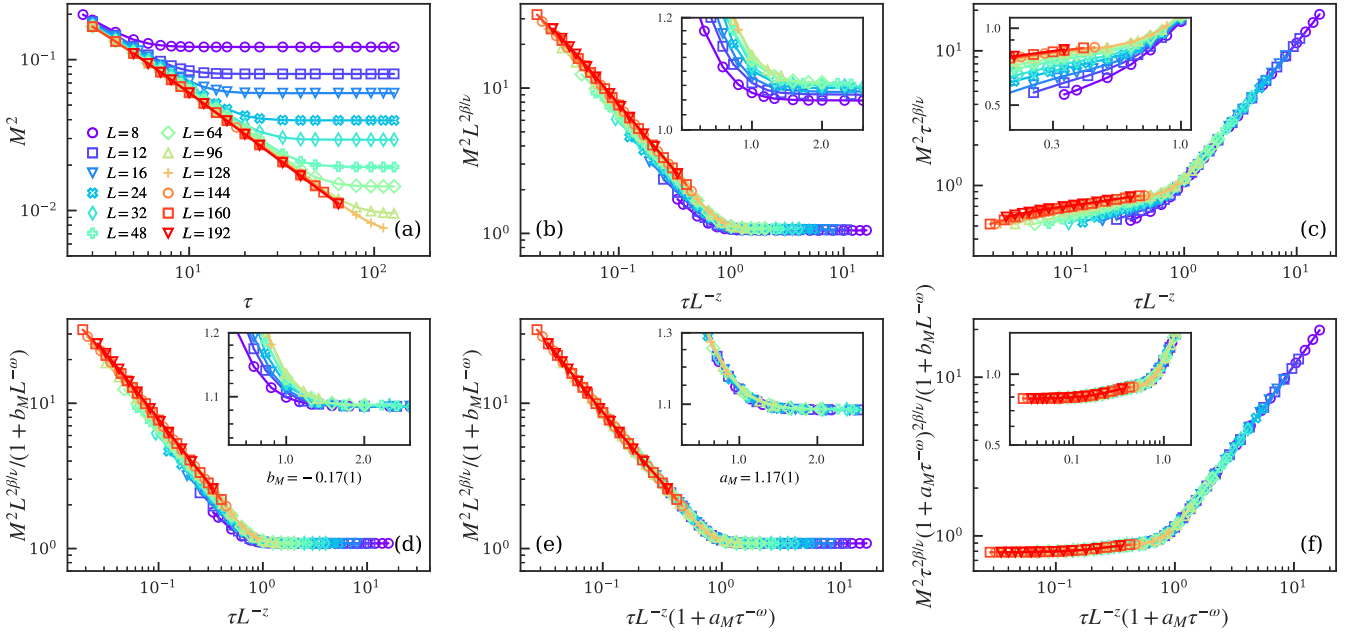


FIG. 3. (a) Evolution of M^2 from the completely ordered AFM initial state for different lattice sizes at the critical point is plotted. Rescaled curves are shown in (b) and (c) according to Eqs. (9) and (7), respectively. Rescaled curves with only finite-size scaling corrections considered are shown in (d). Rescaled curves according to Eqs. (18) and (19), respectively, in which both short-time and finite-size scaling corrections are added. All insets show the details of the scaling collapse. Here both $\beta/\nu = 0.5185$ and $\omega = 0.78$ [76,77] are set as input. Double-logarithmic scales are used.

described by Eq. (1). In particular, in Fig. 2(c), both the correction exponents ω_τ and ω_L are chosen as $\omega = 0.78$, which is analytically obtained in Ref. [77] and numerically verified in Ref. [19], confirming $\omega_\tau = \omega_L$ and the discussion below Eq. (12).

The evolution of M^2 for different system sizes is shown in Fig. 3(a). By rescaling M^2 and τ as $M^2 L^{2\beta/\nu}$ and τL^{-z} according to Eq. (9), we find in Fig. 3(b) that the rescaled curves in the short-time stage have apparent discrepancies despite their tendency to approach each other. The discrepancy is also observed in the equilibrium region, as shown in the inset of Fig. 3(b). Furthermore, as shown in Fig. 3(c), the rescaled curves of $M^2 \tau^{2\beta/\nu}$ versus τL^{-z} according to Eq. (7) also exhibit discrepancies, particularly in the short-time and small-size regions. Moreover, Fig. 3(c) also shows that the rescaled curves in the short-time stage are not parallel to the horizontal axis, even for large system size, demonstrating that the scaling relation of Eq. (8) does not give a complete description of the short-time scaling behavior of M^2 . Accordingly, scaling corrections are needed to improve the dynamic scaling theory discussed in Sec. III A.

A natural question is whether these scaling discrepancies can be eliminated by standard finite-size scaling corrections. To examine it, Fig. 3(d) shows the results when only the finite-size scaling correction is introduced. We find that for $b_M = -0.17(1)$ the rescaled curves match quite well in the long-time stage. However, the curves still deviate from each other in the short-time stage. Thus, an independent short-time scaling correction is required.

Figure 3(e) shows the results when both short-time and finite-size scaling corrections are included according to

Eq. (18). By tuning the coefficient a_M before $\tau^{-\omega}$, while fixing the coefficient b_M before $L^{-\omega}$ to the same value as in Fig. 3(d), the results show that for $a_M = 1.17(1)$ the rescaled curves of $M^2 L^{2\beta/\nu}$ versus τL^{-z} can collapse quite well over the whole relaxation process.

In addition, by substituting the obtained a_M and b_M values into Eq. (19) and rescaling the data according to this equation, we find that the rescaled curves also collapse quite well, as shown in Fig. 3(f). These results not only successfully verify the effectiveness of scaling forms of Eqs. (18) and (19), but also determine the coefficient of the short-time scaling correction. Moreover, in Fig. 3(f), the rescaled curves in the short-time stage are mainly parallel to the abscissa axis, demonstrating again that appropriate scaling corrections have been established.

To further reveal the short-time dynamic scaling behavior of M^2 , in Fig. 4, we directly fit the curve of M^2 versus τ for large system size $L = 192$ according to Eq. (20) with the critical exponents set as input. We find that the prefactor a_M before $\tau^{-\omega}$, determined from this fitting is $a_M = 1.28(2)$, which is close to that obtained from data collapse in Fig. 3. Accordingly, we not only confirm that in the short-time stage, the evolution of M^2 satisfies Eq. (20), but also verify the value of a_M .

C. Disordered initial state

Next, we investigate the imaginary-time relaxation critical dynamics starting from the completely disordered initial state. This initial state can be regarded as the high-temperature thermal state, as illustrated in Fig. 1. We focus on the critical dynamics of M^2 .

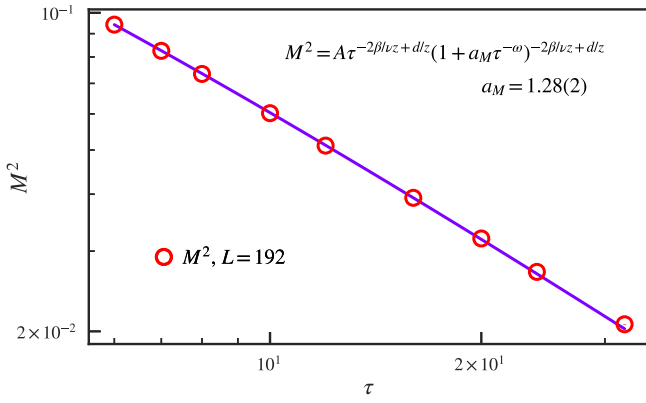


FIG. 4. Dependence of M^2 on the evolution imaginary time τ with the ordered initial state for $L = 192$ at the critical point. Power-law fitting according to Eq. (20) gives $a_M = 1.28(2)$. Here both $\beta/\nu = 0.5185$ and $\omega = 0.78$ [76,77] are set as input. Double-logarithmic scales are used.

Figure 5(a) shows the evolution of M^2 for different system sizes. Different from the decay behavior observed for the ordered initial state, here M^2 increases as τ increases. Furthermore, in the short-time stage and for large L , where the correlation length is smaller than the lattice size, $M^2 \propto L^{-d}$. Thus, when plotting $M^2 L^d$, we find that in the short-time and large-size regions, the curves collapse onto each other. This reflects that the relation of $M^2 \propto L^{-d}$ does not require any scaling correction, as it is a direct result of the central limit theorem, as discussed in Sec. III B.

We then rescale M^2 and τ for different system sizes according to the finite-size scaling form without scaling corrections, i.e., Eq. (9), and show the results in Fig. 5(b). From Fig. 5(b) and its inset, one finds that apparent separations appear in the short-time and small-size regions. The discrepancies in the short-time stage are more obvious when M^2 is rescaled according to Eq. (10), as shown in Fig. 5(c). Furthermore, Fig. 5(c) demonstrates that in the short-time regime, the evolution of M^2 does not satisfy Eq. (11) since the rescaled curves are not parallel to the horizontal axis. Accordingly, scaling corrections are needed.

In addition, Fig. 5(d) shows that the finite-size scaling correction can remedy the scaling mismatching in the long-time equilibrium regime. However, the discrepancy still exists in the short-time regime.

These results motivate us to incorporate both short-time and finite-size scaling corrections, similar to the previous case with an ordered initial state. In Fig. 5(e), we rescale the curves of M^2 versus τ for different sizes according to Eq. (18), then tune the coefficient a_M of the short-time correction term $\tau^{-\omega}$ with b_M fixed as its equilibrium value, i.e., $b_M = -0.17(1)$. We find in Fig. 5(e) that for $a_M = 0.94(3)$, the rescaled curves for different system sizes collapse quite well in the entire relaxation process, confirming the availability of Eq. (18). Furthermore, here the value of the prefactor a_M is noticeably different from the one for the ordered initial state, demonstrating that this coefficient depends on the initial state.

In addition, with the obtained a_M and b_M , we rescale the data according to Eq. (21) and find that the rescaled curves also collapse quite well, as shown in Fig. 5(f). These results successfully verify the effectiveness of the short-time scal-

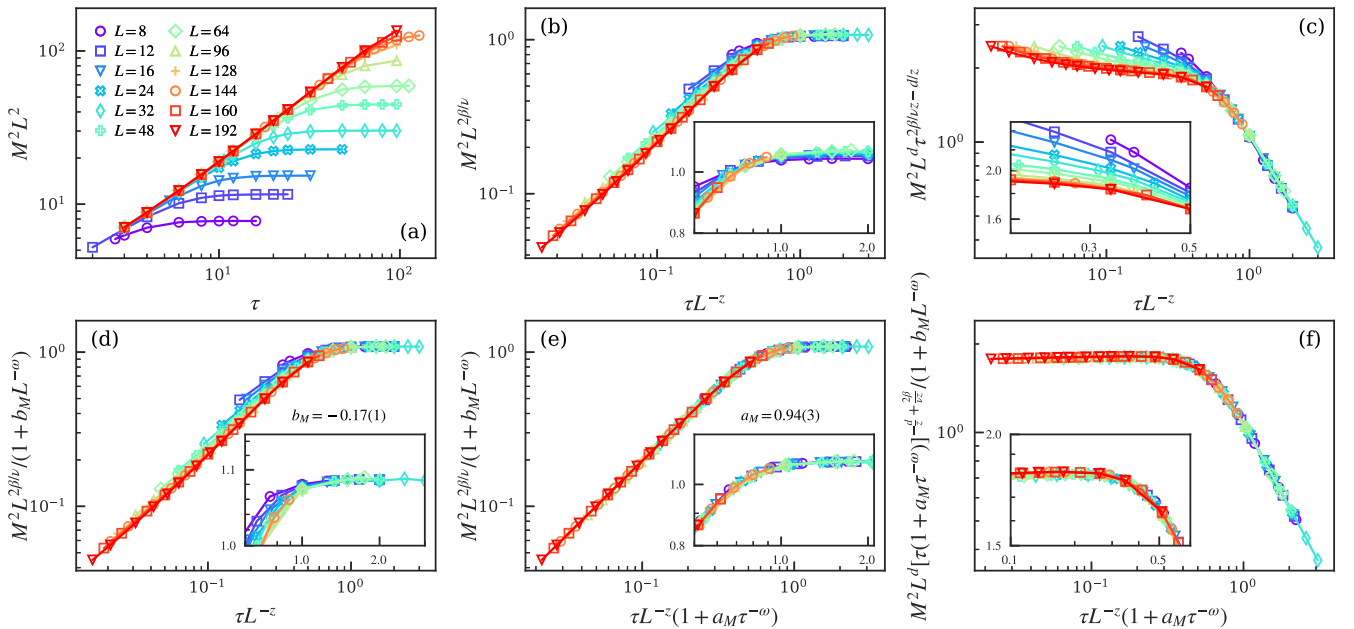


FIG. 5. (a) Evolution of M^2 from the completely disordered initial state for different lattice sizes at the critical point is plotted. Rescaled curves are shown in (b) and (c) according to Eqs. (9) and (10), respectively. Rescaled curves with only finite-size scaling corrections considered are shown in (d). Rescaled curves according to Eqs. (18) and (21), respectively, in which both short-time and finite-size scaling corrections are added. All insets show the details of the scaling collapse. Here both of $\beta/\nu = 0.5185$ and $\omega = 0.78$ [76,77] are set as input. Double-logarithmic scales are used.

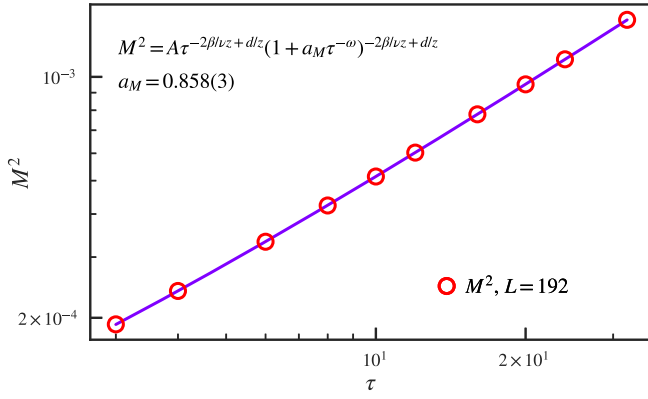


FIG. 6. Dependence of M^2 on the evolution imaginary time τ with the disordered initial state for $L = 192$ at the critical point. Power-law fitting according to Eq. (22) gives $a_M = 0.858(3)$. Here both of $\beta/\nu = 0.5185$ and $\omega = 0.78$ [76,77] are set as input. Double-logarithmic scales are used.

ing corrections in Eqs. (18) and (21). Moreover, as shown in Fig. 5(f), the rescaled curves almost keep aclinic in the short-time regime, demonstrating again that appropriate scaling corrections have been introduced.

To further reveal the short-time dynamic scaling behavior of M^2 , we directly fit the curve of M^2 versus τ for large size $L = 192$ according to Eq. (22) with the critical exponents set as input. We find in Fig. 6 that the prefactor of the short-time correction obtained from this fitting is $a_M = 0.858(3)$, close to the value obtained from data collapse in Fig. 5. Accordingly, we not only show that in the short-time stage, the evolution

of M^2 satisfies Eq. (22), but also confirm the value of the coefficient of the short-time correction.

D. Paramagnetic initial state

In this section, we turn to investigate the evolution of M^2 from the quantum PM initial state, as shown in Fig. 1. This PM state is also magnetically disordered with zero magnetization. Therefore, we expect the scaling behaviors of M^2 to be analogous to those observed in Sec. IV C.

Figure 7(a) shows the evolution of M^2 for different system sizes. Apparent discrepancies can be found in the rescaled curves when they are rescaled using the scaling functions (9) and (10) without scaling corrections, as shown in Figs. 7(b) and 7(c). With only finite-size scaling correction included, Fig. 7(d) demonstrates that the discrepancy still exists in the short-time region.

As shown in Figs. 7(e) and 7(f), by rescaling the curves of M^2 versus τ for different sizes according to Eqs. (18) and (21), respectively, the rescaled curves for different sizes collapse well in the whole relaxation process when the prefactor a_M in the short-time correction is chosen as $a_M = 0.41(2)$. These results confirm the universality of the scaling forms of Eqs. (18) and (21). Moreover, as shown in Fig. 7(f), the rescaled curves almost keep parallel to the horizontal axis in the short-time stage, demonstrating again that appropriate scaling corrections have been built.

The short-time dynamic scaling behavior of M^2 with the PM initial state is further explored in Fig. 8. Therein we directly fit the curve of M^2 versus τ for large size $L = 192$ according to Eq. (22) with the critical exponents set as input. We find that the short-time correction prefactor is

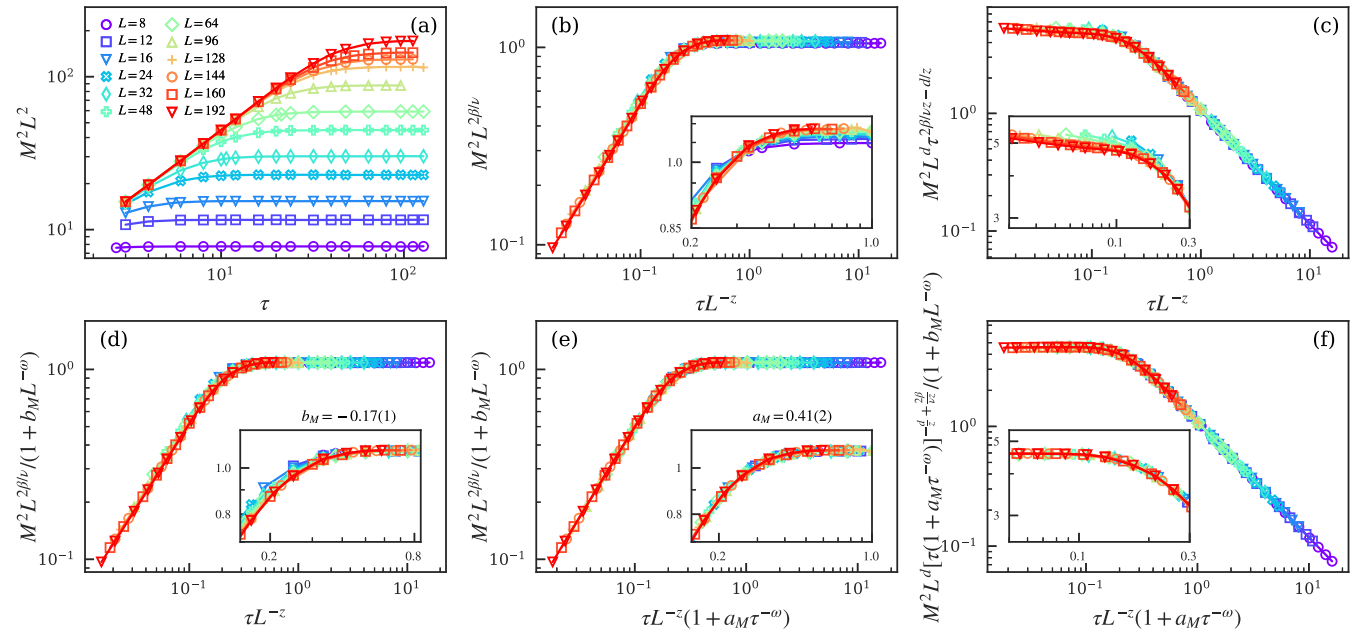


FIG. 7. (a) Evolution of M^2 from the quantum PM initial state for different lattice sizes at the critical point is plotted. Rescaled curves are shown in (b) and (c) according to Eqs. (9) and (10), respectively. Rescaled curves with only finite-size scaling corrections considered are shown in (d). Rescaled curves according to Eqs. (18) and (21), respectively, in which both short-time and finite-size scaling corrections are added. All insets show the details of the scaling collapse. Here both of $\beta/\nu = 0.5185$ and $\omega = 0.78$ [76,77] are set as input. Double logarithmic scales are used.

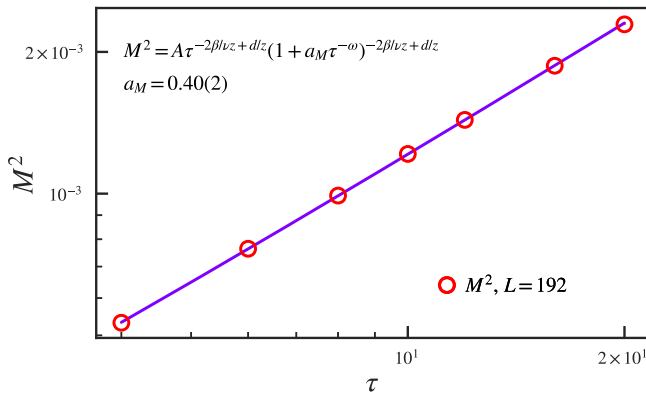


FIG. 8. Dependence of M^2 on the evolution imaginary time τ with the PM initial state for $L = 192$ at the critical point. Power-law fitting according to Eq. (22) gives $a_M = 0.40(2)$. Here both of $\beta/\nu = 0.5185$ and $\omega = 0.78$ [76,77] are set as input. Double-logarithmic scales are used.

$a_M = 0.40(2)$, close to that obtained from data collapse in Fig. 7. Accordingly, we not only show that in the short-time stage, the evolution of M^2 satisfies Eq. (21), but also confirm the value of a_M .

V. SUMMARY

In summary, we have studied the imaginary-time relaxation dynamics in the 2D dimerized Heisenberg model. Our results indicate that the conventional scaling forms fail to accurately describe the critical imaginary-time relaxation behaviors in

this model. Moreover, we have found that aside from the finite-size scaling correction, an additional short-time scaling correction is required to be included in the dynamic scaling theory. A full scaling form, including both short-time and finite-size scaling corrections, has been proposed. From this scaling form, improved short-imaginary-time relaxation scaling properties have been obtained. We have then verified these full scaling forms and short-time scaling properties through QMC simulations for different initial states. Note that the imaginary-time dynamics have been realized experimentally in the platforms of quantum computers to prepare the ground state of quantum systems [60–62]. In particular, the short-imaginary-time scaling behavior has also been found in these systems [70]. Thus, it is expected that our results could be verified in the near-term quantum devices. Moreover, although the real-time dynamics have a unitary nature, which is distinct from the dissipative nature of imaginary-time dynamics, both real and imaginary times share the same scaling dimension [35,39–42]. Therefore, it is expected that the real-time critical dynamics can have similar correction forms.

ACKNOWLEDGMENTS

J.-Q.C., X.-Q.R., and S.Y. are supported by the National Natural Science Foundation of China (Grants No. 12075324 and No. 12222515). S.Y. is also supported by the Science and Technology Projects in Guangdong Province (Grant No. 2021QN02X561). Y.-R.S. is supported by the National Natural Science Foundation of China, Grant No. 12104109, and Key Discipline of Materials Science and Engineering, Bureau of Education of Guangzhou, Grant No. 202255464.

- [1] S. Sachdev, *Quantum Phase Transitions*, 2nd ed. (Cambridge University Press, Cambridge, 2011).
- [2] S. L. Sondhi, S. M. Girvin, J. P. Carini, and D. Shahar, Continuous quantum phase transitions, *Rev. Mod. Phys.* **69**, 315 (1997).
- [3] S. Chakravarty, B. I. Halperin, and D. R. Nelson, Low-temperature behavior of two-dimensional quantum antiferromagnets, *Phys. Rev. Lett.* **60**, 1057 (1988).
- [4] R. R. P. Singh, M. P. Gelfand, and D. A. Huse, Ground states of low-dimensional quantum antiferromagnets, *Phys. Rev. Lett.* **61**, 2484 (1988).
- [5] R. R. P. Singh, Thermodynamic parameters of the $T = 0$, spin-1/2 square-lattice Heisenberg antiferromagnet, *Phys. Rev. B* **39**, 9760(R) (1989).
- [6] A. J. Millis and H. Monien, Spin gaps and spin dynamics in $\text{La}_{2-x}\text{Sr}_x\text{CuO}_4$ and $\text{YBa}_2\text{Cu}_3\text{O}_{7-\delta}$, *Phys. Rev. Lett.* **70**, 2810 (1993).
- [7] A. V. Chubukov, S. Sachdev, and J. Ye, Theory of two-dimensional quantum Heisenberg antiferromagnets with a nearly critical ground state, *Phys. Rev. B* **49**, 11919 (1994).
- [8] M. Troyer, H. Kontani, and K. Ueda, Phase diagram of depleted Heisenberg model for CaV_4O_9 , *Phys. Rev. Lett.* **76**, 3822 (1996).
- [9] J.-K. Kim and M. Troyer, Low temperature behavior and crossovers of the square lattice quantum Heisenberg antiferromagnet, *Phys. Rev. Lett.* **80**, 2705 (1998).
- [10] M. Matsumoto, C. Yasuda, S. Todo, and H. Takayama, Ground-state phase diagram of quantum Heisenberg antiferromagnets on the anisotropic dimerized square lattice, *Phys. Rev. B* **65**, 014407 (2001).
- [11] L. Wang, K. S. D. Beach, and A. W. Sandvik, High-precision finite-size scaling analysis of the quantum-critical point of $S = 1/2$ Heisenberg antiferromagnetic bilayers, *Phys. Rev. B* **73**, 014431 (2006).
- [12] T. Giamarchi, C. Rüegg, and O. Tchernyshyov, Bose-Einstein condensation in magnetic insulators, *Nat. Phys.* **4**, 198 (2008).
- [13] S. Sachdev, Quantum magnetism and criticality, *Nat. Phys.* **4**, 173 (2008).
- [14] A. W. Sandvik, Computational studies of quantum spin systems, *AIP Conf. Proc.* **1297**, 135 (2010).
- [15] P. Merchant, B. Normand, K. W. Krämer, M. Boehm, D. F. McMorrow, and Ch. Rüegg, Quantum and classical criticality in a dimerized quantum antiferromagnet, *Nat. Phys.* **10**, 373 (2014).
- [16] M. Lohöfer, T. Coletta, D. G. Joshi, F. F. Assaad, M. Vojta, S. Wessel, and F. Mila, Dynamical structure factors and excitation modes of the bilayer Heisenberg model, *Phys. Rev. B* **92**, 245137 (2015).
- [17] S. Wenzel, L. Bogacz, and W. Janke, Evidence for an unconventional universality class from a two-dimensional dimerized quantum Heisenberg model, *Phys. Rev. Lett.* **101**, 127202 (2008).

- [18] Y. Q. Qin, B. Normand, A. W. Sandvik, and Z. Y. Meng, Multiplicative logarithmic corrections to quantum criticality in three-dimensional dimerized antiferromagnets, *Phys. Rev. B* **92**, 214401 (2015).
- [19] N. Ma, P. Weinberg, H. Shao, W. Guo, D.-X. Yao, and A. W. Sandvik, Anomalous quantum-critical scaling corrections in two-dimensional antiferromagnets, *Phys. Rev. Lett.* **121**, 117202 (2018).
- [20] J. Wu, W. Yang, C. Wu, and Q. Si, Quantum critical dynamics for a prototype class of insulating antiferromagnets, *Phys. Rev. B* **97**, 224405 (2018).
- [21] D.-R. Tan, C.-D. Li, and F.-J. Jiang, Classification for the universal scaling of Néel temperature and staggered magnetization density of three-dimensional dimerized spin- $\frac{1}{2}$ antiferromagnets, *Phys. Rev. B* **97**, 094405 (2018).
- [22] D.-R. Tan and F.-J. Jiang, Universal scaling of three-dimensional dimerized quantum antiferromagnets on bipartite lattices, *Phys. Rev. B* **101**, 054420 (2020).
- [23] A. W. Sandvik and D. J. Scalapino, Order-disorder transition in a two-layer quantum antiferromagnet, *Phys. Rev. Lett.* **72**, 2777 (1994).
- [24] H. M. Rønnow, D. F. McMorrow, R. Coldea, A. Harrison, I. D. Youngson, T. G. Perring, G. Aeppli, O. Syljuåsen, K. Lefmann, and C. Rischel, Spin dynamics of the 2D spin $\frac{1}{2}$ quantum antiferromagnet copper deuterioformate tetradeuterate (CFTD), *Phys. Rev. Lett.* **87**, 037202 (2001).
- [25] E. Manousakis, The spin- $\frac{1}{2}$ Heisenberg antiferromagnet on a square lattice and its application to the cuprous oxides, *Rev. Mod. Phys.* **63**, 1 (1991).
- [26] H. Löhneysen, A. Rosch, M. Vojta, and P. Wölfle, Fermi-liquid instabilities at magnetic quantum phase transitions, *Rev. Mod. Phys.* **79**, 1015 (2007).
- [27] A. Polkovnikov, K. Sengupta, A. Silva, and M. Vengalattore, *Colloquium: Nonequilibrium dynamics of closed interacting quantum systems*, *Rev. Mod. Phys.* **83**, 863 (2011).
- [28] J. Dziarmaga, Dynamics of a quantum phase transition and relaxation to a steady state, *Adv. Phys.* **59**, 1063 (2010).
- [29] D. M. Stamper-Kurn and M. Ueda, Spinor Bose gases: Symmetries, magnetism, and quantum dynamics, *Rev. Mod. Phys.* **85**, 1191 (2013).
- [30] L. D'Alessio, Y. Kafri, A. Polkovnikov, and M. Rigol, From quantum chaos and eigenstate thermalization to statistical mechanics and thermodynamics, *Adv. Phys.* **65**, 239 (2016).
- [31] A. Mitra, Quantum quench dynamics, *Annu. Rev. Condens. Matter Phys.* **9**, 245 (2018).
- [32] N. Tsuji, M. Eckstein, and P. Werner, Nonthermal antiferromagnetic order and nonequilibrium criticality in the Hubbard model, *Phys. Rev. Lett.* **110**, 136404 (2013).
- [33] L. M. Sieberer, S. D. Huber, E. Altman, and S. Diehl, Dynamical critical phenomena in driven-dissipative systems, *Phys. Rev. Lett.* **110**, 195301 (2013).
- [34] M. Heyl, A. Polkovnikov, and S. Kehrein, Dynamical quantum phase transitions in the transverse-field Ising model, *Phys. Rev. Lett.* **110**, 135704 (2013).
- [35] S.-K. Jian, S. Yin, and B. Swingle, Universal prethermal dynamics in Gross-Neveu-Yukawa criticality, *Phys. Rev. Lett.* **123**, 170606 (2019).
- [36] S. Yin and S.-K. Jian, Fermion-induced dynamical critical point, *Phys. Rev. B* **103**, 125116 (2021).
- [37] J. Berges, M. P. Heller, A. Mazeliauskas, and R. Venugopalan, QCD thermalization: Ab initio approaches and interdisciplinary connections, *Rev. Mod. Phys.* **93**, 035003 (2021).
- [38] J. Berges, S. Borsányi, and C. Wetterich, Prethermalization, *Phys. Rev. Lett.* **93**, 142002 (2004).
- [39] A. Chiochetta, M. Tavora, A. Gambassi, and A. Mitra, Short-time universal scaling in an isolated quantum system after a quench, *Phys. Rev. B* **91**, 220302(R) (2015).
- [40] C. B. Dağ, Y. Wang, P. Urich, X. Na, and J. C. Halimeh, Critical slowing down in sudden quench dynamics, *Phys. Rev. B* **107**, L121113 (2023).
- [41] J. Marino, M. Eckstein, M. S. Foster, and A. M. Rey, Dynamical phase transitions in the collisionless pre-thermal states of isolated quantum systems: theory and experiments, *Rep. Prog. Phys.* **85**, 116001 (2022).
- [42] M.-R. Li and S.-K. Jian, Quantum electrodynamics under a quench, [arXiv:2312.13531](https://arxiv.org/abs/2312.13531).
- [43] L. W. Clark, L. Feng, and C. Chin, Universal space-time scaling symmetry in the dynamics of bosons across a quantum phase transition, *Science* **354**, 606 (2016).
- [44] K. Du, X. Fang, C. Won, C. De, F.-T. Huang, W. Xu, H. You, F. J. Gómez-Ruiz, A. del Campo, and S.-W. Cheong, Kibble-Zurek mechanism of Ising domains, *Nat. Phys.* **19**, 1495 (2023).
- [45] N. Navon, A. L. Gaunt, R. P. Smith, and Z. Hadzibabic, Critical dynamics of spontaneous symmetry breaking in a homogeneous Bose gas, *Science* **347**, 167 (2015).
- [46] G. Lamporesi, S. Donadello, S. Serafini, F. Dalfovo, and G. Ferrari, Dynamics of a quantum phase transition in a ferromagnetic Bose-Einstein condensate, *Nat. Phys.* **9**, 656 (2013).
- [47] E. Nicklas, M. Karl, M. Höfer, A. Johnson, W. Muessel, H. Strobel, J. Tomkovič, T. Gasenzer, and M. K. Oberthaler, Observation of scaling in the dynamics of a strongly quenched quantum gas, *Phys. Rev. Lett.* **115**, 245301 (2015).
- [48] P. Jurcevic, H. Shen, P. Hauke, C. Maier, T. Brydges, C. Hempel, B. P. Lanyon, M. Heyl, R. Blatt, and C. F. Roos, Direct observation of dynamical quantum phase transitions in an interacting many-body system, *Phys. Rev. Lett.* **119**, 080501 (2017).
- [49] P. Weinberg, M. Tylutki, J. M. Rönkkö, J. Westerholm, J. A. Åström, P. Manninen, P. Törmä, and A. W. Sandvik, Scaling and diabatic effects in quantum annealing with a D-wave device, *Phys. Rev. Lett.* **124**, 090502 (2020).
- [50] M. Dupont and J. E. Moore, Quantum criticality using a superconducting quantum processor, *Phys. Rev. B* **106**, L041109 (2022).
- [51] A. D. King, J. Raymond, T. Lanting, R. Harris, A. Zucca, F. Altomare, A. J. Berkley, K. Boothby, S. Ejtemaee, C. Enderud, E. Hoskinson, S. Huang, E. Ladizinsky, A. J. R. MacDonald, G. Marsden, R. Molavi, T. Oh, G. Poulin-Lamarre, M. Reis, C. Rich *et al.*, Quantum critical dynamics in a 5,000-qubit programmable spin glass, *Nature (London)* **617**, 61 (2023).
- [52] G. Semeghini, H. Levine, A. Keesling, S. Ebadi, T. T. Wang, D. Bluvstein, R. Verresen, H. Pichler, M. Kalinowski, R. Samajdar, A. Omran, S. Sachdev, A. Vishwanath, M. Greiner, V. Vuletić, and M. D. Lukin, Probing topological spin liquids on a programmable quantum simulator, *Science* **374**, 1242 (2021).
- [53] S. Ebadi, T. T. Wang, H. Levine, A. Keesling, G. Semeghini, A. Omran, D. Bluvstein, R. Samajdar, H. Pichler, W. W. Ho, S. Choi, S. Sachdev, M. Greiner, V. Vuletić, and M. D. Lukin,

- Quantum phases of matter on a 256-atom programmable quantum simulator, *Nature (London)* **595**, 227 (2021).
- [54] G. Vidal, Efficient simulation of one-dimensional quantum many-body systems, *Phys. Rev. Lett.* **93**, 040502 (2004).
- [55] G. Vidal, Classical simulation of infinite-size quantum lattice systems in one spatial dimension, *Phys. Rev. Lett.* **98**, 070201 (2007).
- [56] J. Jordan, R. Orús, G. Vidal, F. Verstraete, and J. I. Cirac, Classical simulation of infinite-size quantum lattice systems in two spatial dimensions, *Phys. Rev. Lett.* **101**, 250602 (2008).
- [57] H. C. Jiang, Z. Y. Weng, and T. Xiang, Accurate determination of tensor network state of quantum lattice models in two dimensions, *Phys. Rev. Lett.* **101**, 090603 (2008).
- [58] F. F. Assaad and H. G. Evertz, World-line and determinantal quantum Monte Carlo methods for spins, phonons and electrons, in *Computational Many-Particle Physics*, edited by H. Fehske, R. Schneider, and A. Weiße (Springer, Berlin, 2008), pp. 277–356.
- [59] Z.-X. Li and H. Yao, Sign-problem-free fermionic quantum Monte Carlo: Developments and applications, *Annu. Rev. Condens. Matter Phys.* **10**, 337 (2019).
- [60] M. Motta, C. Sun, A. T. K. Tan, M. J. O’Rourke, E. Ye, A. J. Minnich, F. G. S. L. Brandão, and G. K.-L. Chan, Determining eigenstates and thermal states on a quantum computer using quantum imaginary time evolution, *Nat. Phys.* **16**, 205 (2020).
- [61] H. Nishi, T. Kosugi, and Y.-i. Matsushita, Implementation of quantum imaginary-time evolution method on NISQ devices by introducing nonlocal approximation, *npj Quantum Inf.* **7**, 85 (2021).
- [62] S.-H. Lin, R. Dilip, A. G. Green, A. Smith, and F. Pollmann, Real- and imaginary-time evolution with compressed quantum circuits, *PRX Quantum* **2**, 010342 (2021).
- [63] S. Yin, P. Mai, and F. Zhong, Universal short-time quantum critical dynamics in imaginary time, *Phys. Rev. B* **89**, 144115 (2014).
- [64] S. Zhang, S. Yin, and F. Zhong, Generalized dynamic scaling for quantum critical relaxation in imaginary time, *Phys. Rev. E* **90**, 042104 (2014).
- [65] Y.-R. Shu, S. Yin, and D.-X. Yao, Universal short-time quantum critical dynamics of finite-size systems, *Phys. Rev. B* **96**, 094304 (2017).
- [66] Y.-R. Shu and S. Yin, Short-imaginary-time quantum critical dynamics in the $J - Q_3$ spin chain, *Phys. Rev. B* **102**, 104425 (2020).
- [67] Y.-R. Shu, S.-K. Jian, and S. Yin, Nonequilibrium dynamics of deconfined quantum critical point in imaginary time, *Phys. Rev. Lett.* **128**, 020601 (2022).
- [68] Y.-R. Shu and S. Yin, Dual dynamic scaling in deconfined quantum criticality, *Phys. Rev. B* **105**, 104420 (2022).
- [69] Y.-K. Yu, Z.-Zeng, Y.-R. Shu, Z.-X. Li, and S. Yin, Nonequilibrium dynamics in Dirac quantum criticality, [arXiv:2310.10601](https://arxiv.org/abs/2310.10601).
- [70] S.-X. Zhang and S. Yin, Universal imaginary-time critical dynamics on a quantum computer, *Phys. Rev. B* **109**, 134309 (2024).
- [71] H. K. Janssen, B. Schaub, and B. Schmittmann, New universal short-time scaling behaviour of critical relaxation processes, *Z. Phys. B* **73**, 539 (1989).
- [72] E. V. Albano, M. A. Bab, G. Baglietto, R. A. Borzi, T. S. Grigera, E. S. Loscar, D. E. Rodriguez, M. L. R. Puzzo, and G. P. Saracco, Study of phase transitions from short-time non-equilibrium behaviour, *Rep. Prog. Phys.* **74**, 026501 (2011).
- [73] Z. B. Li, L. Schülke, and B. Zheng, Dynamic Monte Carlo measurement of critical exponents, *Phys. Rev. Lett.* **74**, 3396 (1995).
- [74] B. Zheng, Generalized dynamic scaling for critical relaxations, *Phys. Rev. Lett.* **77**, 679 (1996).
- [75] A. Sushcheyev and S. Wessel, Anomalous scaling corrections and quantum phase diagram of the Heisenberg antiferromagnet on the spatially anisotropic honeycomb lattice, *Phys. Rev. B* **108**, 235146 (2023).
- [76] M. Campostrini, M. Hasenbusch, A. Pelissetto, P. Rossi, and E. Vicari, Critical exponents and equation of state of the three-dimensional Heisenberg universality class, *Phys. Rev. B* **65**, 144520 (2002).
- [77] R. Guida and J. Zinn-Justin, Critical exponents of the N -vector model, *J. Phys. A: Math. Gen.* **31**, 8103 (1998).
- [78] A. W. Sandvik and H. G. Evertz, Loop updates for variational and projector quantum Monte Carlo simulations in the valence-bond basis, *Phys. Rev. B* **82**, 024407 (2010).